DATA PAPER

Theoretical study of electron-impact broadening for highly charged Ar XV ion lines

Chao Wu(吴超)[1], Xiang Gao(高翔)[1,†], Yu-Hao Zhu(朱宇豪)[1,4,‡], Xiao-Ying Han(韩小英)[1], Bin Duan(段斌)[1], Ju Meng(孟举)[1], Song-Bin Zhang(张松斌)[3], Jun Yan(颜君)[1,2], Yong Wu(吴勇)[1,2,§], and Jian-Guo Wang(王建国)[1]

[1] *National Key Laboratory of Computational Physics, Institute of Applied Physics and Computational Mathematics, Beijing* 100088, *China*
[2] *HEDPS, Center for Applied Physics and Technology, Peking University, Beijing* 100084, *China*
[3] *School of Physics and Information Technology, Shaanxi Normal University, Xi'an* 710119, *China*
[4] *School of Science, Xi'an University of Architecture and Technology, Xi'an* 710055, *China*

(Received 22 December 2022; revised manuscript received 18 January 2023; accepted manuscript online 31 January 2023)

Spectral line widths produced by collisions between charged particles and emitters are of special interest for precise plasma spectroscopy. The highly charged Ar XV ion is demonstrated to have strong intrashell electron interactions, which manifest as an atomic system with many resonance structures, due to the quasi-degeneracy of orbital energies. In this paper we use the relativistic R-matrix method to investigate the electron-impact broadening of highly charged Ar XV ion spectral lines under the impact approximation. It is found that the results considering resonance structures are significantly different from those of the distorted wave approach. Furthermore, we propose a new empirical formula with a correction term to take into account the effect of resonances for electron-impact widths over a relatively wide range of plasma conditions. The corresponding fitting parameters of the new empirical formula for all 47 calculated transitions are also given with an estimated accuracy within 1%, which should be convenient for practical applications. The dataset that supported the findings of this study is available in Science Data Bank, with the link https://doi.org/10.57760/sciencedb.j00113.00101.

Keywords: highly charged ions, electron-impact broadening, empirical formula

PACS: 31.10.+z, 31.15.ag, 34.80.Bm **DOI:** 10.1088/1674-1056/acb769

1. Introduction

Generally, radiation damping of an excited atom or ion leads to the broadening of spectral lines. In plasmas, the microfield of surrounding ions perturbs the radiating ions by the Stark effect and leads to so-called Stark broadening.[1] Similarly, the high-speed electrons also perturb the emitting ions through collisions and cause the interruption of spontaneous emission. This interruption will broaden the widths of the emission lines, and is known as electron-impact broadening. Electron-impact broadening plays important roles in plasma diagnostics,[2] and is also an essential atomic parameter in opacity calculations.[3] Therefore, investigations on electron-impact broadening are crucial for research programs in astrophysics and controlled fusion research.

Argon is one of the most abundant heavy elements and exists widely in various plasma environments, including planetary nebulae, stellar atmospheres, interstellar media and fusion plasmas.[4] With the development of satellite-borne spectrograph and space astronomy, the spectral lines of argon ions with different degrees of ionization were detected and applied in hot stars and white dwarfs.[5–9] Plenty of emission lines from highly charged Ar XV ions have been observed and applied in astrophysical, tokamak and other laboratory plasmas.[7,10–18] For example, the line intensity ratios and line widths of Ar XV ion were used to diagnose plasma level population and electron density.[19] The line widths of Ar XV ions are also required in spectrum simulations.[20]

For the above-mentioned plasmas with relatively low electron densities, the impact approximation theory (IAT) is applicable. This was first formulated by Baranger[21] and later reviewed by Griem.[1] The theory considers a single binary collision between a perturber and a perturbed ion. During the time of electron collision with a radiating ion, the interaction between perturbing ions is ignored and at any time each electron interacts with only one perturbed ion. The width and shift of a spectral line are linearly proportional to electron density N_e and depend on the scattering matrix for binary collisions. In practice, the scattering matrix for the IAT can be obtained from either the semiempirical formula[22] or quantum mechanical methods.[23,24] The reliability of quantum mechanical methods under the distorted wave approximation for the IAT has been reported previously, where the effect of resonant electron-capture processes was not considered.[25] For near-neutral ions, these resonant processes generally occur in low-energy regions. With the statistical convolution of the electron velocity distribution for considering the finite plasma

[†]Corresponding author. E-mail: gao_xiang@iapcm.ac.cn
[‡]Corresponding author. E-mail: zhu_yuhao@foxmail.com
[§]Corresponding author. E-mail: wu_yong@iapcm.ac.cn

© 2023 Chinese Physical Society and IOP Publishing Ltd

temperature, the influence of these resonant processes should be negligible. On the other hand, for highly ionized ions, the weight contributed by the lower-energy region will be greatly increased at the same temperature due to the Z^2 scaling of the electron energy. In addition, the electron orbitals tend to become hydrogen-like due to the dominant strong Coulomb interaction from the nuclear charge. Such threshold quasi-degeneracy would produce dense resonance structures in collision processes.[26]

An Ar XV ion can be regarded as a highly ionized ion.[26] Fernández-Menchero[27] used the frame transformation R-matrix method to calculate only the electron collision strengths of Be-like ions, and the relativistic effect was not strictly considered. Additionally, previous investigations on Ar XV line broadening only used the semiclassical perturbation method[28] and the nonrelativistic distorted wave approach,[29] in which the contribution of resonance structures to electron-impact broadening was not included. Furthermore, the available Ar XV electron-impact line broadening data were scarce. It is therefore of great significance to consider the effect of resonance structures and provide more reliable electron-impact line broadening data for the Ar XV ion.

In the present work, we have carried out relativistic quantum mechanical close-coupling calculations on the electron-impact processes of the Ar XV ion based on the Dirac atomic R-matrix code (DARC).[30] The electron-impact broadening based on the IAT under different plasma conditions is obtained. For the important range of temperatures in the application, we found that the results considering resonance structures are significantly different from those of distorted waves. It is very interesting to find that the results of electron-impact broadening by considering the resonance structures for all 47 calculated transitions can be represented by a universal fitting formula with respect to the variations of electron temperature and density. We thus propose a new empirical formula for electron-impact widths over a relatively wide range of plasma conditions. The corresponding fitting parameters of the new empirical formula for all 47 calculated transitions are given, with an estimated accuracy within 1%, which should be convenient for practical applications.

This paper is organized as follows. In Section 2, the theoretical methods used to calculate electron-impact broadening are described. Section 3 presents the line broadening results and discusses relevant fitting formulae. A short summary is given in Section 4.

2. Theoretical methods

For ions in plasmas, the total power $P(\omega)$ emitted at energy $\hbar\omega$ in a radiative transition from the initial state α to the final state β can be expressed as

$$P(\omega) = \frac{2\hbar\omega^3 e^2}{m_e c^3} N_A g_\alpha f_{\alpha\beta} L(\omega), \tag{1}$$

with e, m_e, and c the electron charge, mass, and speed of light as the usual convention. $g_\alpha f_{\alpha\beta}$ is the weighted oscillator strength, N_A the ion density of the plasma and $L(\omega)$ the normalized profile factor, which is a Lorentzian for electron-impact broadening

$$L(\omega) = \frac{w_{\alpha\beta}/2\pi}{(\omega - \overline{\omega_{\alpha\beta}})^2 + w_{\alpha\beta}^2/4}, \tag{2}$$

with $w_{\alpha\beta}$ the line width and $\overline{\omega_{\alpha\beta}}$ the radiative transition energy including the tiny shift induced by electron collisions.

In a plasma condition with relatively low electron density and moderate temperature, the time interval between strong collisions is much longer than the duration of such collisions. Then we can view each electron interaction only with one perturbed ion at a time, where all detailed interactions can be embodied in scattering matrices. Under these circumstances, Baranger[21] developed the IAT to calculate the $w_{\alpha\beta}$, in which the time-dependent fluctuating interaction of the electrons with the ions was replaced by a constant non-Hermitian effective interaction composed by scattering matrix elements corresponding to the initial and final states of the radiative transition of the perturbed ion. The scattering matrices can be calculated by quantum mechanical methods, such as the distorted wave method[31] and close-coupling method.[30,32] These quantum mechanical methods have been used in the study of electron-impact broadening.[3,23,33–35] The impact broadening parameters calculated by the IAT with different quantum mechanical methods are different due to the different precisions of the scattering matrices. For example, the distorted wave method generally does not consider resonant structures, while the close-coupling method can accurately describe resonant structures. In this paper, the full relativistic close-coupling R-matrix method is adopted, which can take into account both the relativistic effect and the resonance structures of low-energy electron collisions in HCI ions, including the present Ar XV ion. We consider the $(N+1)$-electron system consisting of an N-electron target ion and an electron. To facilitate later discussions, we denote by J_m^T the total angular momentum of the N-electron target state Φ_m, (l, j) is the orbital and total angular momentum of the scattering electron and $J_m\pi$ is the total angular momentum and parity of the $(N+1)$-electron system formed by the target m and the scattering electron (l, j). In the R-matrix calculations, J_m^T, l, j, and J_m are regarded as channels in the close-coupling expansions. The more channel expansions that are considered in the calculation, the more convergent the results would be. With the calculated scattering matrix $S_E^{J\pi}$ at the energy E, we can

obtain the electron collision excitation strength $\Omega_{\alpha\beta}$ between the atom states $J_\alpha^{\rm T}$ and $J_\beta^{\rm T}$[36]

$$\Omega_{\alpha\beta} = \sum_{J\pi} \frac{2J+1}{2} \sum_{jj',ll'} |S_E^{J\pi}(J_\alpha^{\rm T} lj, J_\beta^{\rm T} l'j')|^2, \tag{3}$$

with $E = E_\alpha^{\rm T} + \varepsilon_\alpha = E_\beta^{\rm T} + \varepsilon_\beta$, ε_α, ε_β the energy of the scattering electron in the corresponding scattering channel and $E_\alpha^{\rm T}$ and $E_\beta^{\rm T}$ the energy of the target ions.

Based on the IAT, the electron-impact broadening (full width at half maximum) of the isolated line transition of target atoms is written as

$$w_{\alpha\beta} = 2N_{\rm e} \left(\frac{\hbar}{m_{\rm e}}\right)^2 \left(\frac{2m_{\rm e}\pi}{k_{\rm B}T_{\rm e}}\right)^{1/2} \times \int_0^\infty \Gamma_{\alpha\beta}(\varepsilon) \exp\left(\frac{-\varepsilon}{k_{\rm B}T_{\rm e}}\right) {\rm d}\left(\frac{\varepsilon}{k_{\rm B}T_{\rm e}}\right), \tag{4}$$

with $N_{\rm e}$ and ε the electron density and electron energy and $T_{\rm e}$ and $k_{\rm B}$ the electron temperature and Boltzmann constant. $\Gamma_{\alpha\beta}$ is the collision strength for electron-impact broadening[24]

$$\begin{aligned}\Gamma_{\alpha\beta}(\varepsilon) = & \sum_{J_\alpha\pi_\alpha J_\beta\pi_\beta jj'll'} (-1)^{2J_\alpha^{\rm T}+2J_\beta+j+j'} \frac{1}{2}(2J_\alpha+1) \\ & \times (2J_\beta+1) \times \left\{ \begin{matrix} J_\beta & J_\alpha & 1 \\ J_\alpha^{\rm T} & J_\beta^{\rm T} & j \end{matrix} \right\} \left\{ \begin{matrix} J_\beta & J_\alpha & 1 \\ J_\alpha^{\rm T} & J_\beta^{\rm T} & j' \end{matrix} \right\} \\ & \times \Big[\delta_{ll'}\delta_{jj'} - {\rm Re}(S^{J_\alpha\pi_\alpha}_{E_\alpha^{\rm T}+\varepsilon}(J_\alpha^{\rm T} l'j', J_\alpha^{\rm T} lj) \\ & \times S^{J_\beta\pi_\beta *}_{E_\beta^{\rm T}+\varepsilon}(J_\beta^{\rm T} l'j', J_\beta^{\rm T} lj)) \Big]. \end{aligned} \tag{5}$$

Note that the two conjugate scattering matrix elements shown in Eq. (5) are on different energy shells, reflecting the impact effects on the initial and final states of the radiative transition process from the colliding electron of the same energy.

3. Computational results and discussion

The DARC relativistic close-coupling R-matrix method[30] is applied in this study to calculate the scattering matrix $S_E^{J\pi}$ in Eqs. (3) and (5). Briefly, based on the partial-wave expansion method, the coupling of N-electron ion core target states Φ_m and an excited electron with the appropriate angular momentum forms channels for the $(N+1)$-electron excited complex with a specific total angular momentum. The multi-channel logarithmic derivative boundary matrix $R_E^{J\pi}$ is obtained by solving the $(N+1)$-electron problem variationally within the R-matrix box, i.e., the reaction zone. With the $R_E^{J\pi}$ matrix, the scattering matrix $S_E^{J\pi}$ can be calculated with the proper outgoing-wave expressions on the boundary of the reaction zone.

For the R-matrix calculation, the quality of target wavefunctions Φ_m as well as the number of target states, which in turn determines the coupled-channel expansions included in the calculation, are crucial to the final convergence of the calculated scattering matrix. In the present work, the GRASP2018 code[37] based on the multi-configuration Dirac–Fock method is used to optimize target wavefunction orbitals of the Ar XV ion. We use the multi-configuration sets ($1s^22s^2$, $1s^22s2p$, $1s^22p^2$, $1s^22s3s$, $1s^22s3p$, $1s^22s3d$, $1s^22p3s$, $1s^22p3p$, $1s^22p3d$, $1s^22s4s$, $1s^22s4p$, $1s^22s4d$, $1s^22s4f$, $1s^22p4s$, $1s2s3d^2$, $1s^23d^2$, $2s^23d^2$, $1s2s2p3d$, $1s2p3d^2$, and $1s2p^3$) as the reference configurations to optimize $1l$, $2l$, $3l$, and $4l$ orbitals. By keeping these optimized spectroscopic orbitals fixed, we carry out the extended-optimal-level calculations to further optimize virtual orbital sets, i.e., $5l$ ($l = 0$–4), $6l$ ($l = 0$–5), $7l$ ($l = 0$–5), $8l$ ($l = 0$–5), and $9l$ ($l = 0$–5), step by step with increasing principal quantum number for electron correlation effects. The respective configurations are generated by all possible single and double excitations from the multi-reference configuration sets to the corresponding virtual orbital sets. With these configurations and optimized orbitals, the target state wavefunctions are obtained by a separate relativistic configuration interaction calculation.[37] Table 1 lists the calculated first 64 fine-structure energy levels of the Ar XV ion connected with configurations of $1s^22s^2$, $1s^22s2p$, $1s^22p^2$, $1s^22s3s$, $1s^22s3p$, $1s^22s3d$, $1s^22p3s$, $1s^22p3p$, $1s^22p3d$, $1s^22s4s$, $1s^22s4p$, $1s^22s4d$, $1s^22s4f$, and $1s^22p4s$, which are used in later R-matrix calculations. As shown in Table 1, our result is in excellent agreement with the experimental data[38] within 0.053%, which is systematically better than previous theoretical results.[39,40] Table 2 exhibits our calculated weighted oscillator strengths ($g_\alpha f_{\alpha\beta}$) and transition probabilities ($A_{\alpha\beta}$ in s^{-1}), together with other theoretical results[39,40] of the radiative E1 transitions from the first five states to $2s3l$ and $2p3l$ states, which are the transitions for the later electron-impact broadening investigations. Our results are in good agreement with those from the literature.[39,40] We have used both the length and velocity forms of the E1 transition operator to calculate $g_\alpha f_{\alpha\beta}$, as the agreement between the results of the two forms is commonly used as an independent criterion for the convergence of the electron correlation effects.[41] As shown in Table 2, the agreement between our calculated $g_\alpha f_{\alpha\beta}^{\rm L}$ and $g_\alpha f_{\alpha\beta}^{\rm V}$ is within 1.8% for all transitions. Therefore, our calculated results shown in Tables 1 and 2 demonstrate the good quality of the target wavefunctions used in our R-matrix calculations for the scattering matrix.

In the scattering calculation, the convergence of partial-wave expansions of the electron collision excitation strength is not exactly the same as that of the collision strength for electron-impact broadening defined in this paper. For example, calculation of the collision strength of the dipole allowed transition requires a large number of partial-wave expansions,

Table 1. The excitation energies (Ryd) of Ar XV levels relative to the ground level.

Index	Conf.	Level	$E_{\rm exp}$[a]	E[b]	$E_{\rm KM}$[c]	$E_{\rm AK}$[d]	Index	Conf.	Level	$E_{\rm exp}$[a]	E[b]	$E_{\rm KM}$[c]	$E_{\rm AK}$[d]
1	$2s^2$	$^1S_0$	0.0000	0.0000	0.0000	0.0000	33	2p3p	$^3P_2$	39.7358	39.7329	39.7397	39.7642
2	2s2p	$^3P^o_0$	2.0838	2.0786	2.0889	2.0885	34	2p3d	$^3F^o_3$	–	39.8131	39.8219	39.8463
3	2s2p	$^3P^o_1$	2.1493	2.1440	2.1542	2.1565	35	2p3d	$^1D^o_2$	39.8634	39.8829	39.8848	39.9106
4	2s2p	$^3P^o_2$	2.3026	2.2972	2.3066	2.3156	36	2p3d	$^3F^o_4$	39.9108	39.9459	39.9541	39.9815
5	2s2p	$^1P^o_1$	4.1209	4.1177	4.1970	4.1909	37	2p3p	$^1P_2$	39.9955	39.9922	40.0208	40.0469
6	$2p^2$	$^3P_0$	5.5128	5.5104	5.5470	5.5515	38	2p3d	$^3D^o_1$	–	40.0911	40.0968	40.1242
7	$2p^2$	$^3P_1$	5.6054	5.6012	5.6381	5.6471	39	2p3d	$^3D^o_2$	–	40.1373	40.1423	40.1696
8	$2p^2$	$^3P_2$	5.7253	5.7220	5.7588	5.7719	40	2p3d	$^3D^o_3$	40.2097	40.2168	40.2209	40.2507
9	$2p^2$	$^1D_2$	6.2843	6.2817	6.3563	6.3731	41	2p3d	$^3P^o_2$	40.3053	40.3078	40.3162	40.3426
10	$2p^2$	$^1S_0$	7.6602	7.6588	7.7921	7.7951	42	2p3d	$^3P^o_1$	–	40.3314	40.3410	40.3649
11	2s3s	$^3S_1$	35.8584	35.8793	35.8607	35.8883	43	2p3d	$^3P^o_0$	–	40.3483	40.3586	40.3787
12	2s3s	$^1S_0$	36.2684	36.2731	36.2603	36.2853	44	2p3p	$^1S_0$	–	40.4570	40.5143	40.5373
13	2s3p	$^1P^o_1$	36.8389	36.8317	36.8287	36.8536	45	2p3d	$^1F^o_3$	40.6607	40.6589	40.7047	40.7355
14	2s3p	$^3P^o_0$	–	36.8537	36.8476	36.8680	46	2p3d	$^1P^o_1$	40.7282	40.7192	40.7611	40.7873
15	2s3p	$^3P^o_1$	–	36.8908	36.8856	36.9075	47	2s4s	$^3S_1$	–	48.0380	48.0177	48.0521
16	2s3p	$^3P^o_2$	36.9109	36.9151	36.9087	36.9290	48	2s4s	$^1S_0$	–	48.1769	48.1629	48.1904
17	2s3d	$^3D_1$	–	37.4364	37.4271	37.4527	49	2s4p	$^3P^o_0$	–	48.4168	48.4025	48.4319
18	2s3d	$^3D_2$	–	37.4442	37.4349	37.4618	50	2s4p	$^3P^o_1$	–	48.4215	48.4078	48.4375
19	2s3d	$^3D_3$	37.4531	37.4570	37.4478	37.4755	51	2s4p	$^3P^o_2$	–	48.4424	48.4281	48.4570
20	2s3d	$^1D_2$	37.8176	37.8229	37.8436	37.8708	52	2s4p	$^1P^o_1$	–	48.4651	48.4576	48.4879
21	2p3s	$^3P^o_0$	–	38.4902	38.4926	38.5165	53	2s4d	$^3D_1$	–	48.6576	48.6413	48.6731
22	2p3s	$^3P^o_1$	–	38.5435	38.5474	38.5720	54	2s4d	$^3D_2$	–	48.6603	48.6441	48.6763
23	2p3s	$^3P^o_2$	–	38.7162	38.7179	38.7442	55	2s4d	$^3D_3$	48.6617	48.6651	48.6489	48.6813
24	2p3s	$^1P^o_1$	–	39.0360	39.0693	39.0901	56	2s4d	$^1D_2$	48.7710	48.7802	48.7782	48.8078
25	2p3p	$^1P_1$	–	39.1264	39.1293	39.1492	57	2s4f	$^3F^o_2$	–	48.8010	48.7899	–
26	2p3p	$^3D_1$	–	39.2877	39.2911	39.3103	58	2s4f	$^3F^o_3$	–	48.8022	48.7911	–
27	2p3p	$^3D_2$	–	39.2977	39.3045	39.3237	59	2s4f	$^3F^o_4$	48.8075	48.8043	48.7932	–
28	2p3p	$^3D_3$	39.4269	39.4559	39.4621	39.4812	60	2s4f	$^1F^o_3$	48.8348	48.8322	48.8252	–
29	2p3p	$^3S_1$	39.5444	39.5570	39.5632	39.5817	61	2p4s	$^3P^o_0$	–	50.4613	50.4600	50.4875
30	2p3p	$^3P_0$	–	39.5781	39.5827	39.6044	62	2p4s	$^3P^o_1$	–	50.4831	50.4849	50.5118
31	2p3p	$^3P_1$	–	39.6842	39.6904	39.7109	63	2p4s	$^3P^o_2$	–	50.6907	50.6883	50.7167
32	2p3d	$^3F^o_2$	–	39.7096	39.7167	39.7384	64	2p4s	$^1P^o_1$	–	50.7525	50.7633	50.7877

a: NIST database,[38] b: this work, c: Aggarwal KM,[39] d: Bhatia AK.[40]

Table 2. The weighted oscillator strengths and transition probabilities (s^{-1}) for intercombination transitions of Ar XV. The number of lower and upper transitions is the index of energy level in Table 1.

Lower (α)	Upper (β)	$g_\alpha f^{\rm V}_{\alpha\beta}$[a]	$g_\alpha f^{\rm L}_{\alpha\beta}$[b]	$g_\alpha f^{\rm AK}_{\alpha\beta}$[c]	$A_{\alpha\beta}$[d]	$A^{\rm KM}_{\alpha\beta}$[e]	$A^{\rm AK}_{\alpha\beta}$[f]
1	3	2.326 − 04	2.333 − 04	2.120 − 04	2.875 + 06	2.660 + 06	2.640 + 06
1	5	2.066 − 01	2.048 − 01	2.093 − 01	9.334 + 09	9.988 + 09	9.334 + 09
1	13	4.495 − 01	4.488 − 01	4.088 − 01	1.632 + 12	1.544 + 12	1.487 + 12
1	15	1.793 − 01	1.788 − 01	2.171 − 01	6.514 + 11	7.245 + 11	7.923 + 11
1	24	2.429 − 02	2.422 − 02	2.850 − 02	9.907 + 10	1.090 + 11	1.167 + 11
1	38	1.407 − 03	1.406 − 03	1.171 − 03	6.074 + 09	5.312 + 09	5.048 + 09
2	11	2.905 − 02	2.908 − 02	2.892 − 02	8.894 + 10	8.916 + 10	8.846 + 10
2	17	7.332 − 01	7.333 − 01	7.314 − 01	2.453 + 12	2.459 + 12	2.452 + 12
2	25	3.496 − 02	3.495 − 02	3.195 − 02	1.284 + 11	1.189 + 11	1.175 + 11
2	26	1.040 − 01	1.040 − 01	1.040 − 01	3.855 + 11	3.915 + 11	3.860 + 11
2	29	6.055 − 02	6.053 − 02	6.027 − 02	2.275 + 11	2.337 + 11	2.269 + 11
2	31	3.201 − 02	3.199 − 02	3.574 − 02	1.212 + 11	1.202 + 11	1.355 + 11
3	11	8.765 − 02	8.778 − 02	8.745 − 02	2.673 + 11	2.681 + 11	2.665 + 11
3	12	2.606 − 05	2.559 − 05	1.838 − 05	2.401 + 08	2.406 + 08	1.721 + 08
3	17	5.482 − 01	5.482 − 01	5.472 − 01	1.827 + 12	1.832 + 12	1.828 + 12
3	18	1.641 + 00	1.641 + 00	1.638 + 00	3.285 + 12	3.291 + 12	3.285 + 12
3	20	1.146 − 03	1.144 − 03	1.205 − 03	2.334 + 09	2.351 + 09	2.473 + 09
3	25	6.596 − 02	6.595 − 02	6.377 − 02	2.415 + 11	2.349 + 11	2.337 + 11
3	26	3.062 − 03	3.061 − 03	4.227 − 03	1.123 + 10	1.455 + 10	1.563 + 10
3	27	2.717 − 01	2.716 − 01	2.683 − 01	6.021 + 11	5.991 + 11	5.956 + 11
3	29	1.610 − 01	1.610 − 01	1.611 − 01	6.033 + 11	6.155 + 11	6.045 + 11

Table 2. Continued.

Lower (α)	Upper (β)	$g_\alpha f_{\alpha\beta}^{\mathrm{V}\,a}$	$g_\alpha f_{\alpha\beta}^{\mathrm{L}\,b}$	$g_\alpha f_{\alpha\beta}^{\mathrm{AK}\,c}$	$A_{\alpha\beta}{}^{d}$	$A_{\alpha\beta}^{\mathrm{KM}\,e}$	$A_{\alpha\beta}^{\mathrm{AK}\,f}$
3	30	1.030 − 01	1.030 − 01	1.032 − 01	1.159 + 12	1.163 + 12	1.164 + 12
3	31	1.577 − 02	1.577 − 02	1.898 − 02	5.956 + 10	5.788 + 10	7.172 + 10
3	33	7.777 − 02	7.773 − 02	8.206 − 02	1.763 + 11	1.798 + 11	1.866 + 11
3	37	7.216 − 03	7.217 − 03	5.261 − 03	1.668 + 10	1.431 + 10	1.215 + 10
4	11	1.481 − 01	1.484 − 01	1.491 − 01	4.479 + 11	4.489 + 11	4.501 + 11
4	17	3.660 − 02	3.659 − 02	3.649 − 02	1.209 + 11	1.212 + 11	1.208 + 11
4	18	5.468 − 01	5.468 − 01	5.460 − 01	1.084 + 12	1.087 + 12	1.085 + 12
4	26	5.728 − 03	5.727 − 03	6.019 − 03	2.099 + 10	2.102 + 10	2.206 + 10
4	27	3.914 − 02	3.913 − 02	4.028 − 02	8.599 + 10	8.600 + 10	8.867 + 10
4	29	2.910 − 02	2.909 − 02	3.794 − 02	1.081 + 11	1.128 + 11	1.412 + 11
4	31	2.582 − 01	2.581 − 01	2.533 − 01	9.660 + 11	9.753 + 11	9.489 + 11
4	33	4.129 − 01	4.128 − 01	4.145 − 01	9.291 + 11	9.369 + 11	9.344 + 11
4	37	1.625 − 02	1.623 − 02	1.299 − 02	3.727 + 10	3.025 + 10	2.974 + 10
5	11	2.459 − 04	2.472 − 04	2.650 − 04	6.682 + 08	6.118 + 08	7.128 + 08
5	12	3.108 − 02	3.117 − 02	3.399 − 02	2.589 + 11	2.762 + 11	2.814 + 11
5	17	1.337 − 03	1.331 − 03	1.279 − 03	3.961 + 09	3.596 + 09	3.793 + 09
5	18	1.469 − 03	1.478 − 03	1.707 − 03	2.632 + 09	2.531 + 09	3.038 + 09
5	20	1.617 + 00	1.617 + 00	1.610 + 00	2.951 + 12	2.991 + 12	2.937 + 12
5	25	1.786 − 01	1.786 − 01	1.970 − 01	5.857 + 11	6.349 + 11	6.446 + 11
5	26	1.599 − 01	1.599 − 01	1.619 − 01	5.298 + 11	5.232 + 11	5.345 + 11
5	27	6.178 − 03	6.183 − 03	5.467 − 03	1.232 + 10	1.153 + 10	1.084 + 10
5	29	3.935 − 02	3.934 − 02	3.798 − 02	1.324 + 11	1.293 + 11	1.274 + 11
5	30	1.288 − 03	1.289 − 03	1.031 − 03	1.307 + 10	1.103 + 10	1.039 + 10
5	31	2.223 − 04	2.227 − 04	3.415 − 04	7.575 + 08	6.987 + 08	1.154 + 09
5	33	4.289 − 02	4.290 − 02	3.607 − 02	8.784 + 10	7.354 + 10	7.335 + 10
5	37	7.809 − 01	7.809 − 01	8.247 − 01	1.613 + 12	1.637 + 12	1.705 + 12

a, b, and d: this work (a, velocity form; b, length form). c and f: Bhatia AK.[40] e: Aggarwal KM.[39]

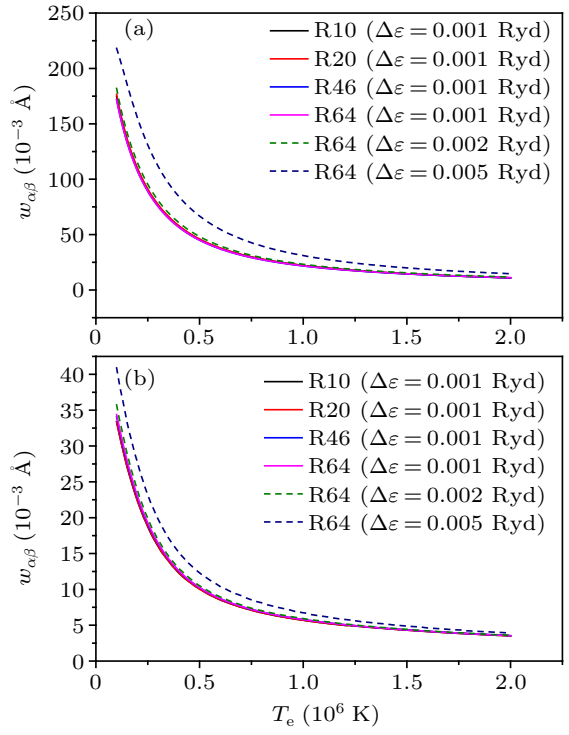


Fig. 1. The electron-impact broadening $w_{\alpha\beta}$ of two Ar XV spectral lines at electron density $N_e = 1 \times 10^{20}$ cm^{-3}: (a) $2s^2\ {}^1S_0$–$2s2p\ {}^3P_1^o$ transition, (b) $2s^2\ {}^1S_0$–$2s2p\ {}^1P_1^o$ transition.

but calculation of the line width only involves the scattering matrix elements of elastic collision of the upper and lower levels, which requires much fewer partial-wave expansions. After checking, we adopted $2J_m \leq 39$ for both parities as adequate for the present line width calculations. We have studied the convergence with respect to the increasing target states. As shown in Fig. 1, we calculated the electron-impact broadening $w_{\alpha\beta}$ of spectral lines using four independent theoretical models, namely: (i) R10, a 10-state calculation including the ground state $2s^2\ {}^1S_0$, as well as the four excited states with configuration 2s2p and the five excited states with configuration $2p^2$; (ii) R20, in addition to (i), we include the 10 states with configuration 2s3*l*; (iii) R46, a 46-state calculation in which the 26 states with configurations 2p3*l* are also included; (iv) R64, compared with (iii), we add 18 states with configuration 2s4*l* and 2p4s. It is evident that the R64 model is convergent, and it is used in all subsequent calculations.

For electron-impact energies below the double-ionization threshold of the Ar XIV ion, the atomic spectra are dominated by a large number of overlapping doubly excited resonance series known as autoionization states. Highly ionized excited states have strong intrashell corrections, resulting in dense resonant structures.[26] Figure 2 shows that the collision excitation strengths $\Omega_{\alpha\beta}$ and the collision strength for electron-impact broadening $\Gamma_{\alpha\beta}$ have a large number of resonance structures under the Ar XV threshold, while the results of the distorted wave calculation with identical target states

using the Flexible Atomic Code (FAC) program[42] do not. These resonant structures can be effectively calculated using multichannel quantum defect theory.[26] As shown in Eq. (4), this paper discusses that electron collision broadening is a convolution result. The more energy grids, the higher the precision of the line widths. It is clearly seen from Fig. 1 that with the reduction of $\Delta\varepsilon$ the line widths calculated by the R64 model show good convergence.

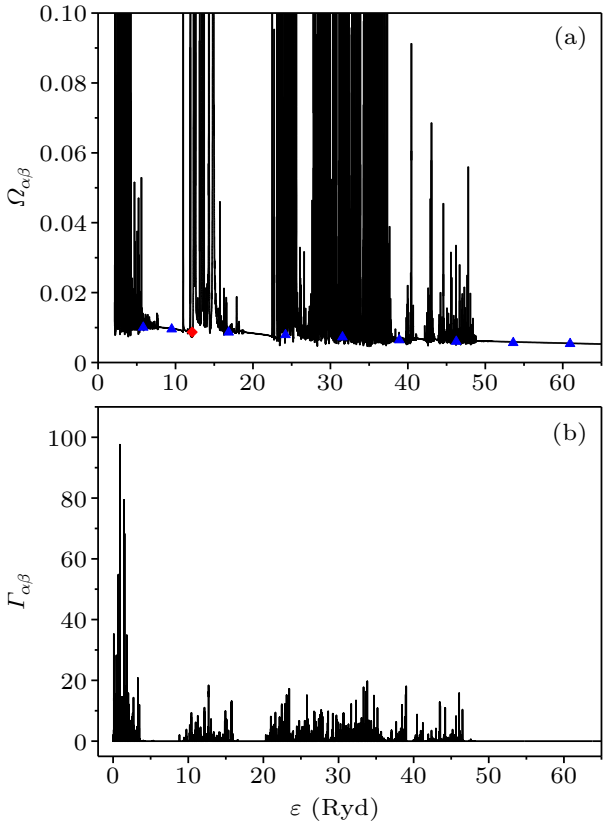


Fig. 2. (a) The collision excitation strength $\Omega_{\alpha\beta}$ of the $2s^2\ {}^1S_0$–$2s2p\ {}^3P^o_1$ transition. (b) The collision strength for electron-impact broadening $\Gamma_{\alpha\beta}$ of the $2s^2\ {}^1S_0$–$2s2p\ {}^3P^o_1$ transition. The blue triangles show distorted wave results using the FAC program and the red rhombus distorted wave results from Elabidi H.[29]

In Table 3 we display $w_{\alpha\beta}$ for four transition lines of Ar XV. The calculations are performed at electron density $N_e = 1\times10^{20}$ cm^{-3}. Moreover, in order to illustrate the variation of the electron-impact broadening with electron temperature in the important range of temperature for applications, the line widths as a function of electron temperature for the four transition lines of Ar XV are displayed in Fig. 3. As shown in both Table 3 and Fig. 3, it is clear that the present results are significantly different from the semiclassical perturbation[28] and distorted wave results.[29] Specifically, the average difference between the present results and the distorted wave and semiclassical perturbation results are 21.6% and 52.0%, respectively. For low-electron-temperature plasmas (1×10^5 K $\le T_e \le 5\times10^5$ K), the electron-impact broadening increases with decrease of the electron temperature and the increasing trend is substantially faster than that of high-electron-temperature plasmas ($T_e > 5\times10^5$ K). At the same time, compared with the present R-matrix results, the distorted wave results show a relatively slow growth trend with decreasing temperature. As shown in Fig. 2(a), although the collision strengths $\Omega_{\alpha\beta}$ of the R-matrix are in good agreement with the distorted wave results in the high-energy region, the rich resonance structures are missing in the distorted wave results for electron incident energies under the Ar XV threshold, which should be the main reason for the differences in $w_{\alpha\beta}$. Therefore, it is necessary to consider the effect of resonance structures on electron-impact broadening, especially in the case of low electron temperature.

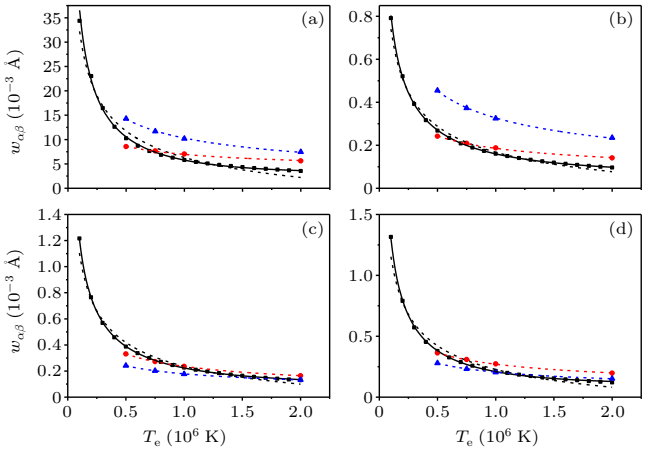


Fig. 3. The electron-impact broadening $w_{\alpha\beta}$ at electron density $N_e = 1\times10^{20}$ cm^{-3} for four Ar XV transitions: (a) $2s^2\ {}^1S_0$–$2s2p\ {}^1P^o_1$, (b) $2s^2\ {}^1S_0$–$2s3p\ {}^1P^o_1$, (c) $2s2p\ {}^3P^o_0$–$2s3s\ {}^3S_1$, (d) $2s2p\ {}^1P^o_1$–$2s3s\ {}^1S_0$. Red circles, distorted wave;[29] blue triangles, semiclassical perturbation;[28] black squares, this work; dotted lines of three colors, fitting by Eq. (7); black solid line, fitting by Eq. (8).

Table 3. The electron-impact broadening $w_{\alpha\beta}$ of Ar XV lines at electron density $N_e = 1\times10^{20}$ cm^{-3}.

Transitions	T_e (10^5 K)	$w_{\alpha\beta}$ [a] (10^{-3} Å)	$w^{dw}_{\alpha\beta}$ [b] (10^{-3} Å)	$w^{scp}_{\alpha\beta}$ [c] (10^{-3} Å)
$2s^2\ {}^1S_0$–$2s2p\ {}^1P^o_1$	5	10.251	8.55	14.3
	7.5	7.224	7.66	11.7
$\lambda = 22.11$ nm	10	5.792	7.04	10.2
	20	3.545	5.62	7.46
$2s^2\ {}^1S_0$–$2s3p\ {}^1P^o_1$	5	0.268	0.242	0.455
	7.5	0.198	0.209	0.373
$\lambda = 2.47$ nm	10	0.159	0.188	0.325
	20	0.096	0.141	0.235
$2s2p\ {}^3P^o_0$–$2s3s\ {}^3S_1$	5	0.387	0.313	0.242
	7.5	0.283	0.273	0.202
$\lambda = 2.69$ nm	10	0.226	0.236	0.177
	20	0.129	0.164	0.133
$2s2p\ {}^1P^o_1$–$2s3s\ {}^1S_0$	5	0.378	0.363	0.380
	7.5	0.272	0.309	0.232
$\lambda = 2.84$ nm	10	0.215	0.273	0.204
	20	0.120	0.197	0.152

a: this work. b: Elabidi.[29] c: Dimitrijević.[28]

Table 4. Fitting coefficients A, B and C with their relative errors (in percent) in $w_{\alpha\beta} = N_e(A + B\ln T_e + C\ln T_e \times T_e^{-1/2})$ for the Ar XV transitions. N_e is in 1×10^{20} cm^{-3}, $w_{\alpha\beta}$ is in 10^{-3} Å and T_e is in K. The number of lower and upper of transitions is the index of energy levels in Table 1.

Lower (α)	Upper (β)	λ (nm)	A	B	C	Error$_A$	Error$_B$	Error$_C$	R^2
1	3	42.397	−718.359	42.345	11237.426	1.19	1.29	0.63	0.9992
1	5	22.113	−136.579	8.116	2188.789	2.01	2.16	1.04	0.9979
1	13	2.474	−2.037	0.118	40.588	0.83	0.84	0.35	0.9998
1	15	2.470	−1.764	0.102	34.172	2.66	2.99	1.10	0.9998
1	24	2.332	−2.527	0.150	39.491	1.14	0.66	0.61	0.9992
1	38	2.273	−0.115	0.006	3.905	5.50	6.39	1.28	0.9998
2	11	2.698	−3.442	0.201	64.262	0.72	0.49	0.32	0.9998
2	17	2.577	0.994	−0.066	4.831	1.61	1.51	2.80	0.9994
2	25	2.460	−5.892	0.357	76.416	5.50	5.60	3.35	0.9979
2	26	2.449	−1.271	0.074	24.485	2.20	2.43	0.89	0.9998
2	29	2.432	−0.936	0.054	19.525	3.09	3.46	1.12	0.9998
2	31	2.423	−0.554	0.031	13.798	3.63	3.14	1.08	0.9998
3	11	2.703	−5.083	0.300	83.989	0.74	0.66	0.38	0.9997
3	12	2.670	−6.534	0.382	109.941	1.65	1.84	0.77	0.9999
3	17	2.582	−0.954	−0.065	6.466	6.07	5.82	7.12	0.9994
3	18	2.581	0.730	−0.051	8.528	6.71	6.15	4.54	0.9996
3	20	2.554	1.334	−0.089	4.297	7.34	6.74	17.92	0.9984
3	25	2.464	−6.244	−0.379	79.973	5.72	6.06	3.52	0.9964
3	26	2.453	−1.358	−0.079	24.988	2.14	2.36	0.91	0.9998
3	27	2.453	−3.411	0.207	46.146	6.15	6.57	3.61	0.9975
3	29	2.436	−0.983	0.057	19.632	2.77	3.04	1.10	0.9998
3	30	2.434	−0.619	−0.036	13.916	4.20	4.63	1.47	0.9997
3	31	2.427	−0.578	0.033	13.583	3.97	4.63	1.38	0.9997
3	33	2.424	0.607	−0.043	38.043	15.9	14.44	1.99	0.9998
3	37	2.407	−1.206	0.072	21.339	5.30	5.74	2.38	0.9994
4	11	2.715	−6.227	0.370	96.051	2.81	2.97	1.43	0.9995
4	17	2.593	1.039	−0.070	5.849	5.77	5.68	8.39	0.9993
4	18	2.593	0.827	−0.057	7.486	6.40	5.94	5.60	0.9995
4	26	2.463	−1.438	0.084	26.077	2.09	2.32	0.92	0.9998
4	27	2.463	−3.523	0.213	47.457	6.13	6.49	3.58	0.9968
4	29	2.446	−1.006	0.058	19.983	2.54	3.03	1.07	0.9998
4	31	2.437	−0.611	0.035	13.967	4.04	4.46	1.38	0.9997
4	33	2.434	−0.396	0.016	53.162	22.72	35.58	1.35	0.9998
4	37	2.417	−1.261	0.075	21.745	5.31	5.76	2.45	0.9989
5	11	2.871	−7.246	0.432	109.789	3.10	3.35	1.61	0.9994
5	12	2.834	−4.627	0.273	76.162	0.99	0.73	0.51	0.9995
5	17	2.735	1.030	−0.070	7.639	6.19	5.82	6.59	0.9994
5	18	2.734	0.801	−0.056	9.252	1.69	6.19	4.54	0.9996
5	20	2.704	1.514	−0.101	3.801	7.32	7.08	23.15	0.9982
5	25	2.603	−6.976	0.424	88.685	1.56	1.07	3.64	0.9969
5	26	2.591	−1.538	0.090	27.812	2.40	2.61	1.04	0.9998
5	27	2.590	−3.830	0.232	50.941	6.47	6.85	3.84	0.9959
5	29	2.572	−1.098	0.064	21.319	3.02	3.29	1.22	0.9997
5	30	2.570	−0.693	0.040	15.084	5.32	5.82	1.92	0.9995
5	31	2.562	−0.642	0.037	14.765	5.29	5.82	1.81	0.9996
5	33	2.558	−0.347	0.017	50.609	57.06	74.56	3.08	0.9994
5	37	2.540	−1.264	0.075	21.895	6.09	6.53	2.76	0.9987

Considering the convenience and diversity of data applications, it is necessary to establish the fitting formula for electron-impact broadening with respect to the electron temperature. The scaling of line widths with electron temperature has been discussed in previous literature. Trklja[43] and Dimitrijević[44] proposed a simple formula of the form

$$w_{\alpha\beta} = N_e(A + BT_e^{-C}). \tag{6}$$

Elabidi[45] later proposed a more physical fitting formula based on the Bethe approximation of electron-impact cross-sections,[46]

$$w_{\alpha\beta} = N_e(A + B\ln T_e \times T_e^{-1/2}). \tag{7}$$

This approximation is valid at high energy and especially good when the difference in energy $E_\beta^T - E_\alpha^T = \hbar\omega$ between the atomic levels of the radiator is small. The reliability of Eq. (7)

is verified by the literature.[45] In Fig. 3, it is noticeable that the fitting accuracy of the present relativistic quantum mechanical calculations according to Eq. (7) is inferior to that of the semi-classical perturbation and distorted wave methods because this approximation is not always effective at low electron energy. Due to the rich resonances missing in the distorted wave results at low electron energy, it seems appropriate to introduce the correction term ($\ln T_e$) into Eq. (7) to take into account the influence of resonance structures under the Ar XV threshold on electron-impact broadening

$$w_{\alpha\beta} = N_e(A + B\ln T_e + C\ln T_e \times T_e^{-1/2}). \tag{8}$$

It is clearly seen from Fig. 3 that the accuracy of the solid line fitted with Eq. (8) for the present results is significantly improved. Finally, the corresponding fitting parameters A, B, C, error and correlation coefficient R^2 of the new empirical formula for all 47 calculated transitions are also given with an estimated accuracy within 1%. Therefore, we believe that the new formula is applicable.

4. Summary

In this work, the electron-impact broadening of transition lines of highly charged Ar XV ions are calculated based on the IAT. The full relativistic close-coupling R-matrix method DARC is used for the scattering matrix required in the IAT, where all resonant structures are included. Compared with the commonly used distorted wave method which does not consider the relevant resonance process, we found that the present line widths have a significant average difference of 21.6% and show a different trend with electron temperature, especially at low electron temperature. Furthermore, we propose an empirical formula of line widths with electron temperature with a correction term to take into account the effect of resonance structures on electron-impact broadening, which is applicable to all 47 transitions in this paper with an estimated accuracy within 1%. We give all the fitting coefficients of these transition lines in Table 4, which should be useful for astrophysical and laboratory applications, especially in plasma parameter diagnostics. As the resonance structures exist widely in other atom systems, we expect that our new fitting formula form should be applicable in general.

Data availability statement

The data that support the findings of this study are openly available in Science Data Bank at https://doi.org/10.57760/sciencedb.j00113.00101.

Acknowledgments

We thank the Institute of Applied Physics and Computational Mathematics for the supercomputing source. Project supported by the National Natural Science Foundation of China (Grant Nos. 11934004, U1832201, and 12241410), the Science Challenge Project (Grant No. TZ2016005), the CAEP Foundation (Grant No. CX2019022), and the Special Innovation Project for National Defense.

References

[1] Griem H R 2012 *Spectral Line Broadening by Plasma* (Elsevier)
[2] Kunze H J 2005 *Plasma Physics*, (Berlin, Heidelberg: Springer) p. 349
[3] Seaton M J 1987 *J. Phys. B: At. Mol. Opt. Phys.* **20** 6431
[4] Lodders K 2003 *Astrophys. J.* **591** 1220
[5] Rauch T, Ziegler M, Werner K and Kruk J W 2007 *Astron. Astrophys.* **470** 317
[6] Werner K, Rauch T and Kruk J W 2007 *Astron. Astrophys.* **466** 317
[7] Purcell J D and Widing K G 1972 *Astrophys. J.* **176** 239
[8] Feldman U, Warren H P, Brown C M, *et al.* 2009 *Astrophys. J.* **695** 36
[9] Doschek G A, Warren H P and Feldman U 2015 *Astrophys. J. Lett.* **808** L7
[10] Whyte D G, Jernigan T C, Humphreys D A, *et al.* 2002 *Phys. Rev. Lett.* **89** 055001
[11] Zhang L, Morita S, Wu Z, *et al.* 2019 *Nucl. Instrum. Meth. A* **916** 169
[12] Nakano T 2015 *J. Nucl. Mater.* **463** 555
[13] Träbert E, Beiersdorfer P, Lepson J K, *et al.* 2018 *Astrophys. J.* **865** 148
[14] Lepson J K, Beiersdorfer P, Behar E, *et al.* 2003 *Astrophys. J.* **590** 604
[15] Magunov A I, Faenov A Y, Skobelev I Y, *et al.* 2002 *J. Exp. Theor. Phys.* **95** 998
[16] Stewart R E, Dietrich D D, Egan P O, *et al.* 1987 *J. Appl. Phys.* **61** 126
[17] Träbert E 1995 *Nucl. Instrum. Meth. B* **98** 10
[18] Khardi S 1994 *Phys. Scripta* **49** 571
[19] KataIi R, Morita S and Goto M 2007 *J. Quant. Spectrosc. Radiat. Transfer* **107** 120
[20] Mattioli M 2001 *J. Phys. B: At. Mol. Opt. Phys.* **34** 127
[21] Baranger M 1958 *Phys. Rev.* **112** 855
[22] Dimitrijević M S and Konjević N 1980 *J. Quant. Spectr. Radiat. Trans.* **24** 451
[23] Elabidi H, Nessib N B and Sahal-Bréchot S 2003 *J. Phys. B: At. Mol. Opt. Phys.* **37** 63
[24] Duan B, Bari M A, *et al.* 2012 *Astron. Astrophys.* **547** A4
[25] Gomez T A, Nagayama T, Fontes C J, *et al.* 2020 *Phys. Rev. Lett.* **124** 055003
[26] Dou L J, Jin R, Sun R, *et al.* 2020 *Phys. Rev. A* **101** 032508
[27] Fernández-Menchero L, Del Z G and Badnell N R 2014 *Astron. Astrophys.* **566** A104
[28] Dimitrijević M S, Kovacevic A, Simic Z, *et al.* 2012 *Publ. Astron. Soc.* **11** 243
[29] Elabidi H, Sahal-Bréchot S and Dimitrijević M S 2014 *Adv. Space Res.* **54** 1184
[30] Ait-Tahar S, Grant I P and Norrington P H 1996 *Phys. Rev. A* **54** 3984
[31] Itikawa Y 1986 *Phys. Rep.* **143** 69
[32] Zhang H L and Pradhan A K 1994 *Phys. Rev. A* **50** 3105
[33] Peach G 1981 *Adv. Phys.* **30** 367
[34] Duan B, Bari M A, Wu Z Q, *et al.* 2012 *Phys. Rev. A* **86** 052502
[35] Duan B, Bari M A, Wu Z Q, *et al.* 2013 *Phys. Rev. A* **87** 032505
[36] Norrington P H and Grant I P 1987 *J. Phys. B: At. Mol. Opt. Phys.* **20** 4869
[37] Fischer C F, *et al.* 2019 *Comput. Phys. Commun.* **237** 184
[38] https://www.nist.gov/pml/atomic-spectra
[39] Aggarwal K M, Keenan F P and Nakazaki S 2005 *Astron. Astrophys.* **436** 1141
[40] Bhatia A K, Feldman U and Seely J F 1986 *Atom. Data Nucl. Data* **35** 449
[41] Han X Y, Gao X, *et al.* 2012 *Phys. Rev. A* **85** 062506
[42] Gu M F 2008 *Can. J. Phys.* **86** 675
[43] Trklja N, Tapalaga I and DojčInović I P 2017 *New Astron.* **59** 54
[44] Dimitrijević M S, *et al.* 2007 *Astron. Astrophys.* **469** 681
[45] Elabidi H and Sahal-Bréchot S 2018 *Mon. Not. R. Astron. Soc.* **480** 697
[46] Bethe H 1957 *Quantum Mechanics of One- and Two-Electron Atoms* (Berlin: Springer-Verlag)